Aspect ratio effect on natural convection in water near its density maximum temperature

Wei Tong

Power Systems Division, General Electric Company, Schenectady, NY 12345, USA

Abstract

The effect of the aspect ratio on natural convection in water subjected to density inversion has been investigated in this study. Numerical simulations of the two-dimensional, steady state, incompressible flow in a rectangular enclosure with a variety of aspect ratios, ranging from 0.125 to 100, have been accomplished using a finite element model. Computations cover Rayleigh numbers from 10^3 to 10^6. Results reveal that the aspect ratio, A, the Rayleigh number, Ra, and the density distribution parameter, R, are the key parameters to determine the heat transfer and fluid flow characteristics for density inversion fluids in an enclosure. A new correlation for predicting the maximum mean Nusselt number is proposed in the form of $\overline{\text{Nu}}_{\max} = a - b \log(A)$, with the constants a and b depending on density distribution number R. It is demonstrated that the aspect ratio has a strong impact on flow patterns and temperature distributions in rectangular enclosures. The stream function ratio $\Psi_{\text{inv}}/|\Psi_{\text{reg}}|$ is introduced to describe quantitatively the interaction between inversional and regular convection. For $R = 0.33$, the density inversion enhancement is observed in the regime near $A = 3$. © 1999 Elsevier Science Inc. All rights reserved.

Keywords: Aspect ratio; Density inversion; Natural convection

Notation

A	aspect ratio, $A = H/L$
a, b	constant
g	gravitational acceleration
H	enclosure height
h	heat transfer coefficient
k	thermal conductivity
L	enclosure width
Nu	Nusselt number, $\text{Nu} = hL/k$
p	pressure
P	dimensionless pressure
Pr	Prandtl number, $\text{Pr} = v/\kappa$
R	density distribution number, $R = (T_0 - T_c)/\Delta T$
Ra	Rayleigh number, $\text{Ra} = g\gamma(\Delta T)^2 L^3/(\kappa v)$
T	temperature
T_0	maximum density temperature of water, 3.98°C
ΔT	temperature difference, $T_h - T_c$
$\mathbf{u}$	velocity vector, $\mathbf{u} = \{u,\ v\}$
$\mathbf{U}$	dimensionless velocity vector, $\mathbf{U} = \{U,\ V\}$
$\mathbf{x}$	coordinate, $\mathbf{x} = \{x,\ y\}$
$\mathbf{X}$	dimensionless coordinate, $\mathbf{X} = \{X,\ Y\}$

Greek

θ	dimensionless temperature
κ	thermal diffusivity
μ	dynamic viscosity
v	kinematic viscosity
ρ	density
ρ_0	maximum density of water at $T_0 = 3.98$°C
ψ	stream function
Ψ	dimensionless stream function

Subscripts

c	cold
h	hot
inv	inversional convection
max	maximum
reg	regular convection
sat	saturation

1. Introduction

Natural convection in a fluid subject to density inversion is important in many engineering and environmental applications such as crystal growth, ice forming and melting, atmospheric and oceanic movements. In the last three decades, numerous studies have focused extensively on convective flows driven by the density inversion effect (Watson, 1972; Seki et al., 1978; Robillard and Vasseur, 1981; Lin and Nansteel, 1987; Ivey and Hamblin, 1989; Lankford and Bejan, 1986; Tong and Koster, 1993, 1994; McDonough and Faghri, 1994; Elkouh and Baliga, 1995). Of particular interest in density inversion

E-mail address: tongwe@pssch.ps.ge.com (W. Tong).

studies is the aspect ratio effect on natural convection in rectangular enclosures. This is because it can provide not only further details of flow and heat transfer characteristics in such fluids, but also a better understanding to physical processes. Although a large number of studies have been devoted to the density inversion problems, the aspect ratio effect has attracted far less attention in the past.

Seki et al. (1978) studied the aspect ratio effect on heat transfer in water including the density inversion influence. They found that for a fixed Rayleigh number the total heat transport reaches its maximum in the range of $0.8 \leqslant A \leqslant 1.5$, according to density distribution number (which is defined in Eq. (1) in this study), and decreases steeply as $A > 1.5$. It was shown that for $R = 0.5$, $\overline{\mathrm{Nu}}$ approaches unity at $A \approx 14$. Ivey and Hamblin (1989) conducted experiments on low aspect ratio cavities at high Rayleigh numbers. Experiments for high aspect ratio cavities were carried out by Lankford and Bejan (1986).

Tong and Koster (1993, 1994) have investigated the aspect ratio effect for both steady state and transient convection. Under steady-state conditions, five aspect ratios ($A = 0.125$, 0.25, 0.5, 1, 2) were investigated at $R = 0.33$ and Ra $= 10^6$. The results have shown that the total heat transfer reaches its maximum at $A = 1$. In the transient convection study, a set of aspect ratios ($A = 0.25$, 0.5, 1, 2, 4, 10) were tested under identical thermal and hydraulic conditions. In all cases, $\overline{\mathrm{Nu}}$ decreases with time and reaches approximately a steady state for dimensionless time $\tau > 300$, at where the heat transfer rate of $A = 1$ is the largest.

The present work is concerned with the aspect ratio effect on natural convection in a density inversion fluid. The aspect ratio investigated in this study is varied from 0.125 to 100, covering a much wider range than those used by previous investigators.

2. Mathematical formulation

Consider water in a rectangular enclosure with two insulated horizontal walls and two isothermal vertical walls heated differently. The enclosure aspect ratio, A, is defined as the ratio of the enclosure height to the width ($A = H/L$). By setting the temperature of the right wall at 0°C and varying the temperature at the left wall at 3.98°C and above, the maximum density surface occurs inside the water layer. Thus, two distinct horizontal liquid sublayers, with opposite density gradients, are formed and separated by this maximum density surface. As a result, convection can initiate and develop from both hot and cold walls, referred to as "regular" and "inversional" convection, respectively (Fig. 1). There is no doubt that in such concurring buoyancy driven flows the temperature and flow fields become more complex in comparison with those in conventional convection systems. To display the location of the maximum density surface more conveniently, the density distribution number, R, is introduced as

$$R = \frac{T_0 - T_c}{\Delta T}, \tag{1}$$

where ΔT is the temperature difference across the cavity width ($\Delta T = T_h - T_c$). Since T_c was set at 0°C in this study, R is in the range $0 < R \leqslant 1$. Note that the case $R = 1$ corresponds to the circumstance in which the hot wall is at temperature T_0 so that fluid density increases monotonically with temperature everywhere in the enclosure.

2.1. Density-temperature relationship of water near its maximum density temperature

It is obvious that the Boussinesq approximation, which is based on a linear variation of density with respect to temper-
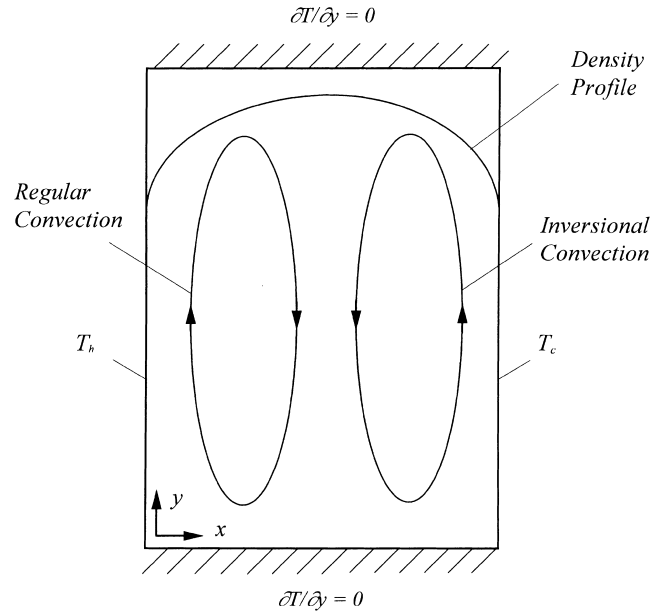

Fig. 1. Schmatic diagram of regular and inversional convection in a density inversion fluid.

ature, is no longer applicable to density inversion fluids. A parabolic-type relationship has been extensively used to calculate water density near its maximum temperature (Delber, 1966; Goren, 1966)

$$\frac{\rho}{\rho_0} = 1.0 - \gamma(T - T_0)^2, \tag{2}$$

where $\gamma = 8.00026 \times 10^{-6}$ (°C)$^{-2}$ and ρ_0 is the maximum density at the temperature T_0.

Besides Eq. (2), a number of density-temperature correlations are also available in the literature (Sun et al., 1969; Fujii, 1974; Wagenbreth and Blanke, 1971; Kell and Whalley, 1975; Gebhart and Mollenderf, 1977). However, the comparison of calculated density ratio ρ/ρ_0 has revealed that within the current temperature range of interest, $0°C \leqslant T \leqslant 12°C$, the relative differences among all these correlations are less than ±0.005%. Due to its concise form, Eq. (2) has been used by many investigators (e.g., Robillard and Vasseur, 1982; Lankford and Bejan, 1986; Tong and Koster, 1993, 1994).

2.2. Governing equations

A natural convective flow in a rectangular enclosure is governed by the continuity, Navier–Stokes, and energy equations. In a two-dimensional coordinate system, the dimensionless governing equations are written as:

$$\nabla \cdot \mathbf{U} = 0, \tag{3}$$

$$\sqrt{\frac{\mathrm{Ra}}{\mathrm{Pr}}}(\mathbf{U} \cdot \nabla \mathbf{U}) = -\nabla P + \nabla^2 \mathbf{U} + \sqrt{\frac{\mathrm{Ra}}{\mathrm{Pr}}} \theta^2 \mathbf{j}, \tag{4}$$

$$\sqrt{\mathrm{Ra}\,\mathrm{Pr}}(\mathbf{U} \cdot \nabla \theta) = \nabla^2 \theta, \tag{5}$$

where $\mathbf{j}$ is the vertical unit vector in the positive Y-coordinate. Eqs. (3)–(5) were nondimensionalized using the following variables:

$$\mathbf{X} = \frac{\mathbf{x}}{L}, \qquad \mathbf{U} = \frac{\mathbf{u}}{\kappa\sqrt{\mathrm{Ra}\,\mathrm{Pr}}/L},$$

$$\theta = \frac{T - T_0}{\Delta T}, \qquad P = \frac{p}{\mu\kappa\sqrt{\mathrm{Ra}\,\mathrm{Pr}}/L^2}, \tag{6}$$

Table 1
Mesh-independence tests at various aspect ratios for $R = 0.33$[a]

A	Mesh	$\overline{Nu}$			
		$Ra = 10^3$	$Ra = 10^4$	$Ra = 10^5$	$Ra = 10^6$
0.20	55×25	1.00000 (0.000)	1.00017 (0.001)	1.01563 (0.006)	1.71719 (0.234)
	75×45	1.00000 (0.000)	1.00016 (0.000)	1.01558 (0.002)	1.71413 (0.065)
	95×65	1.00000 (−)	1.00016 (−)	1.01557 (−)	1.71302 (−)
1.0	25×25	1.01687 (0.001)	1.58285 (0.101)	3.31907 (0.488)	6.61657 (2.550)
	45×45	1.01686 (0.000)	1.58144 (0.011)	3.30267 (0.009)	6.49159 (0.612)
	65×65	1.01685 (−)	1.58126 (−)	3.30030 (−)	6.45208 (−)
30.0	25×121	1.00415 (0.065)	1.08486 (0.147)	1.68215 (0.299)	3.02658 (1.179)
	45×151	1.00368 (0.018)	1.08378 (0.047)	1.67866 (0.092)	3.01752 (0.876)
	65×181	1.00350 (−)	1.08327 (−)	1.67713 (−)	2.99130 (−)

[a] A number in parentheses is the relative difference from the finest mesh value in percentage (%).

where Ra and Pr are the Rayleigh and Prandtl number, respectively

$$Ra = \frac{g\gamma(\Delta T)^2 L^3}{\kappa v}, \quad Pr = \frac{v}{\kappa}. \qquad (7)$$

From Eq. (4), it can be seen that the buoyancy effect is characterized by $\sqrt{Ra/Pr}$.

The isothermal and adiabatic boundary conditions are set at the vertical and horizontal walls, respectively. No-slip boundary conditions are applied to all solid surfaces

$$\mathbf{U} = 0; \quad \theta = \theta_h \text{ at } X = 0,$$
$$\mathbf{U} = 0; \quad \theta = \theta_c \text{ at } X = 1, \qquad (8)$$
$$\mathbf{U} = 0; \quad \frac{\partial \theta}{\partial Y} = 0 \text{ at } Y = 0, A.$$

The effect of the aspect ratio on the temperature and convective flow fields will be addressed separately.

3. Numerical methodology

The nonlinear governing Eqs. (3)–(5) were discretized using a finite element based code *FIDAP*, which is the general purpose code for simulating a wide range of fluid flow and heat transfer problems (Fluid Dynamics International, 1995).

A number of mesh-independence tests were carried out at $A = 0.20$, 1, and 30 under $R = 0.33$. For each aspect ratio, three nonuniform meshes were applied in the test. The relative differences in $\overline{Nu}$ due to different meshes are found rather small for all cases (see Table 1). For instance, for $A = 30$ when the mesh reduces from 65×181 to 25×121 (~70% reduction in the number of meshes), the maximum relative difference is only 1.18%. This indicates that the meshes used in this analysis, as given in Table 2, are suitable.

The iterative Newton–Raphson method was applied in this work. The iteration was terminated as the following convergence criteria were satisfied:

$$\frac{\|\Delta S_i\|}{\|S_i\|} \leqslant \varepsilon_S, \qquad (9)$$

$$\frac{\|R_i(S_i)\|}{\|R_0\|} \leqslant \varepsilon_F, \qquad (10)$$

where $\|\cdot\|$ denotes Euclidean norm, S_i and $R(S_i)$ are the solution vector and residual vector at iteration i, respectively, ε_S and ε_F are small quantities and set to 10^{-4} in this study. The combination of these two checks can provide an effective overall convergence criterion for all occurring situations.

Table 2
Meshes used in the present study

A	Mesh	A	Mesh
0.125	85×45	1.5	45×65
0.15	85×45	2.0	45×75
0.20	75×45	3.0	45×85
0.25	65×45	4.0	45×95
0.30	65×45	6.0	45×101
0.40	65×45	10.0	45×121
0.50	55×45	15.0	45×131
0.65	55×45	30.0	45×151
0.80	55×45	50.0	45×181
1.0	45×45	100.0	45×265
1.1	45×45		

To ensure solution convergence at each load level, the incremental loading strategy was employed in calculations. By this strategy, the first computation starts at a very low Rayleigh number. Then, the solution vectors (temperature, velocity, etc.) from the first execution are used as the initial guess for the next Ra number, and the procedure is repeated until a desired Ra number is reached. Essentially, this incremental approach can be thought of as a more efficient way of implementing a Newton-based method. All computations were executed on an HP-9000/315 workstation.

4. Results and discussion

Heat transfer performance is characterized by Nusselt number, Nu. Under the constant temperature condition, Nu can be expressed in terms of dimensionless variables

$$Nu = \left| \frac{\partial \theta}{\partial X} \right|_{X=0, X=1}. \qquad (11)$$

The mean Nusselt number $\overline{Nu}$ is a measure of the convective heat transfer rates across the two vertical surfaces and is obtained by integrating local Nusselt number Nu along the enclosure height:

$$\overline{Nu} = \frac{1}{A} \int_0^A \left| \frac{\partial \theta}{\partial X} \right|_{X=0, X=1} dY. \qquad (12)$$

From Eq. (12), it can be seen that $\overline{Nu}$ depends upon aspect ratio A. The calculated heat transfer and fluid flow results under various R are given in Table 3.

4.1. Effect of aspect ratio on heat transfer

The variations of $\overline{Nu}$ versus A are presented in Fig. 2(a)–(c) for $R = 1.0$, 0.5 and 0.33, respectively. At very low aspect ratios ($A \sim 0.1$), because of the reduced effective buoyancy force, $\overline{Nu} \equiv 1$, indicating that the main heat transfer mode is conduction. Increasing A will lead to an increase in $\overline{Nu}$ until it reaches its maximum value. Beyond this peak point, a small increase in A will cause the sharp decrease in $\overline{Nu}$ due to the enhanced shear stress effect. At very large A, $\overline{Nu}$ approaches unity for all Rayleigh numbers.

It is seen that for a given A and Ra, the relationship $\overline{Nu}_{R=1} > \overline{Nu}_{R=0.33} > \overline{Nu}_{R=0.5}$ always holds. This is because for $R = 1$ only a unicellular convective roll cell is generated from the cold wall. As R decreases to 0.5, the density gradient becomes symmetric with respect to the enclosure vertical centerline, two counter rotating cells are formed from both hot and cold walls. Hence, an additional thermal resistance between two cells is introduced. For $R = 0.33$, the roll cell developed from the hot wall becomes dominant and the second roll cell shrinks into the right-bottom corner. With a short interface, the thermal resistance becomes smaller than that in the $R = 0.5$ case.

Fig. 2 shows the dependence of $\overline{Nu}$ on the aspect ratio under various density distribution numbers. The maximum mean Nusselt number $\overline{Nu}_{max}$ at each R varies inversely with A, and can be predicted from the following correlation

$$\overline{Nu}_{max} = a - b \log(A), \tag{13}$$

where a and b are constants depending on R (Table 4). To find the possible maximum value of A, Eq. (13) is rewritten as

$$A = 10^{(a - \overline{Nu}_{max})/b}. \tag{14}$$

A reaches its maximum when $\overline{Nu}_{max} = 1$ (see Fig. 2), i.e.,

$$A_{max} = 10^{(a-1)/b}. \tag{15}$$

This gives the upper bound of A in Eq. (13): for $R = 0.5$, $A_{max} \approx 1$; for $R = 1$ and $R = 0.33$, A_{max} becomes 1.7704 and 1.6541, respectively.

One of the interesting results in this study is the aspect ratio effect on the local Nusselt number along vertical walls. The variations of Nu, as a function of Y/H, are displayed in Fig. 3 for $R = 0.33$ under different Ra values. For very small aspect ratios (e.g., $A = 0.15$), because the primary heat transfer mode is conduction, Nu ≈ 1 for all Ra. Increasing A to 1, the heat transfer rate increases remarkably above the wall mid-height in a reflecting S shape. The maximum heat fluxes occur approximately at $Y/H \approx 0.9$ (see Fig. 3(c), (d)). For $A \gg 1$ the Nu curve becomes more smooth and displays a monotonic behavior at the top wall region. The maximum values occur at
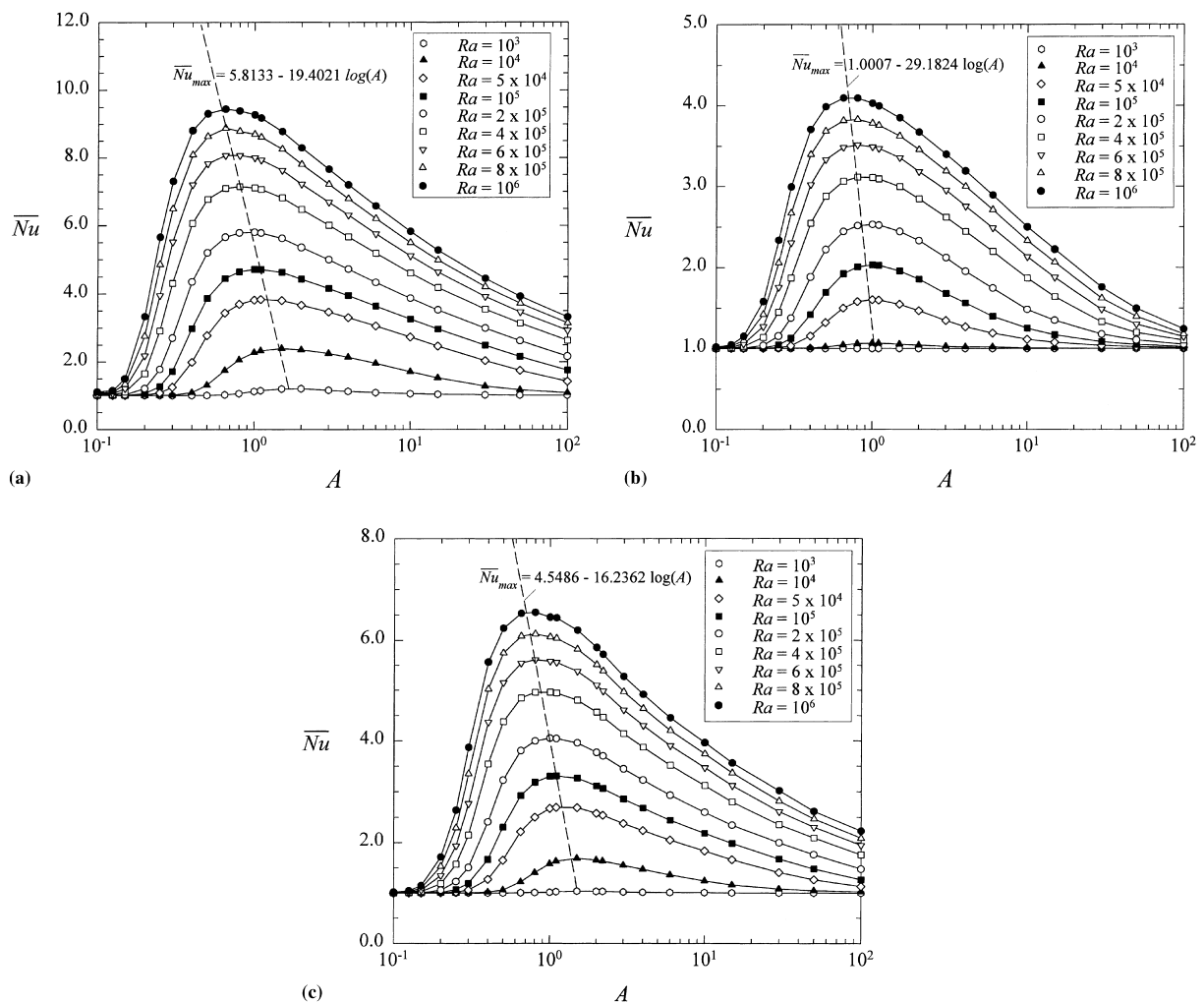

Fig. 2. Aspect ratio effect on heat transfer: (a) $R = 1$; (b) $R = 0.5$; (c) $R = 0.33$.

Table 3
Flow and heat transfer characteristics

A	Ra = 10³			Ra = 10⁴			Ra = 10⁵			Ra = 10⁶		
	$\overline{Nu}$	Ψ_{inv} (× 10³)	Ψ_{reg} (× 10³)	$\overline{Nu}$	Ψ_{inv} (× 10³)	Ψ_{reg} (× 10³)	$\overline{Nu}$	Ψ_{inv} (× 10³)	Ψ_{reg} (× 10³)	$\overline{Nu}$	Ψ_{inv} (× 10³)	Ψ_{reg} (× 10³)
(a) R = 1												
0.125	1.0000	0	−0.0102	1.0000	0	−0.0322	1.0017	0	−0.1017	1.1482	0	−0.2823
0.15	1.0000	0	−0.0205	1.0001	0	−0.0649	1.0070	0	−0.2037	1.4971	0	−0.4967
0.20	1.0000	0	−0.0612	1.0006	0	−0.1935	1.0590	0	−0.5792	3.3270	0	−1.0804
0.25	1.0000	0	−0.1415	1.0034	0	−0.4459	1.2618	0	−1.1810	5.6586	0	−1.6769
0.30	1.0001	0	−0.2771	1.0128	0	−0.8663	1.7175	0	−1.9584	7.3030	0	−2.1981
0.40	1.0010	0	−0.7793	1.0901	0	−2.3061	2.9778	0	−3.6345	8.8098	0	−3.0707
0.50	1.0045	0	−1.6778	1.3040	0	−4.3768	3.8653	0	−5.1579	9.3054	0	−3.7716
0.65	1.0216	0	−3.9103	1.7440	0	−7.9253	4.4512	0	−7.1002	9.4432	0	−4.5723
0.80	1.0578	0	−6.8690	2.0629	0	−11.309	4.6466	0	−8.6644	9.3904	0	−5.1621
1.0	1.1186	0	−10.960	2.2739	0	−15.306	4.7143	0	−10.431	9.2742	0	−5.8519
1.1	1.1447	0	−12.823	2.3263	0	−17.071	4.7128	0	−11.164	9.1764	0	−6.2228
1.5	1.1959	0	−18.089	2.3968	0	−22.865	4.6287	0	−13.843	8.7800	0	−7.7900
2.0	1.2034	0	−21.178	2.3561	0	−29.206	4.4312	0	−18.080	8.2934	0	−10.276
3.0	1.1588	0	−23.540	2.2514	0	−36.852	4.1571	0	−24.805	7.6566	0	−14.110
4.0	1.1234	0	−24.273	2.1412	0	−42.786	3.9431	0	−31.402	7.1999	0	−17.452
6.0	1.0835	0	−24.520	1.9562	0	−51.649	3.6346	0	−43.352	6.5694	0	−23.606
10.0	1.0506	0	−24.533	1.7062	0	−62.402	3.2534	0	−62.921	5.8220	0	−34.710
15.0	1.0343	0	−24.522	1.5196	0	−69.436	2.9615	0	−82.099	5.2764	0	−50.026
30.0	1.0179	0	−24.516	1.2756	0	−75.817	2.4878	0	−121.54	4.4474	0	−80.147
50.0	1.0111	0	−24.482	1.1662	0	−76.817	2.1593	0	−154.62	3.9248	0	−126.76
100.0	1.0059	0	−24.403	1.0833	0	−76.550	1.7505	0	−199.37	3.3179	0	−198.65
(b) R = 0.5												
0.125	1.0000	0.0087	−0.0087	1.0000	0.0274	−0.0274	1.0013	0.0865	−0.0865	1.1124	0.2508	−0.2508
0.15	1.0000	0.0087	−0.0087	1.0000	0.0274	−0.0274	1.0013	0.0865	−0.0865	1.1124	0.2508	−0.2508
0.20	1.0000	0.0244	−0.0244	1.0001	0.0771	−0.0771	1.0099	0.2419	−0.2419	1.5801	0.5669	−0.5669
0.25	1.0001	0.0529	−0.0529	1.0005	0.1671	−0.1671	1.0435	0.5132	−0.5132	2.3341	0.9266	−0.9266
0.30	1.0000	0.0965	−0.0965	1.0015	0.3050	−0.3050	1.1256	0.8943	−0.8943	2.9922	1.2725	−1.2725
0.40	1.0001	0.2348	−0.2348	1.0075	0.7395	−0.7395	1.4176	1.8562	−1.8562	3.7078	1.9503	−1.9503
0.50	1.0002	0.4262	−0.4262	1.0203	1.3323	−1.3323	1.6941	2.8465	−2.8465	3.9834	2.6371	−2.6371
0.65	1.0005	0.7255	−0.7255	1.0439	2.2403	−2.2403	1.9209	4.1525	−4.1525	4.0904	3.5274	−3.5274
0.80	1.0007	0.9746	−0.9746	1.0596	2.9982	−2.9982	2.0066	5.2691	−5.2691	4.0907	4.3924	−4.3924
1.0	1.0007	1.1945	−1.1945	1.0655	3.6263	−3.6263	2.0298	6.3930	−6.3930	4.0272	5.3257	−5.3257
1.1	1.0007	1.2581	−1.2581	1.0645	3.8370	−3.8370	2.0233	6.8512	−6.8512	3.9938	5.7612	−5.7612
1.5	1.0006	1.3648	−1.3648	1.0536	4.2646	−4.2646	1.9568	8.3028	−8.3028	3.8485	7.3446	−7.3446
2.0	1.0004	1.3741	−1.3741	1.0413	4.3710	−4.3710	1.8543	9.6255	−9.6255	3.6727	9.6322	−9.6322
3.0	1.0003	1.3755	−1.3755	1.0277	4.4066	−4.4066	1.6749	11.241	−11.241	3.3969	12.530	−12.530
4.0	1.0002	1.3754	−1.3754	1.0208	4.4052	−4.4052	1.5621	12.372	−12.372	3.1890	15.047	−15.047
6.0	1.0001	1.3755	−1.3755	1.0209	4.4014	−4.4014	1.3957	12.986	−12.986	2.8900	18.832	−18.832
10.0	1.0001	1.3755	−1.3755	1.0083	4.4058	−4.4058	1.2488	13.760	−13.760	2.4998	24.281	−24.281
15.0	1.0001	1.3755	−1.3755	1.0055	4.4025	−4.4025	1.1616	13.837	−13.837	2.2206	29.064	−29.064
30.0	1.0000	1.3754	−1.3754	1.0028	4.4069	−4.4069	1.0845	13.854	−13.854	1.7577	37.012	−37.012
50.0	1.0000	1.3752	−1.3752	1.0017	4.4057	−4.4057	1.0513	13.865	−13.865	1.4950	39.741	−39.741
100.0	1.0000	1.3748	−1.3748	1.0008	4.3985	−4.3985	1.0260	13.875	−13.875	1.2413	41.477	−41.477

(c) $R = 0.33$

0.125	1.0000	0.0025	-0.0063	1.0000	0.0080	-0.0201	1.0005	0.0254	-0.0634	1.0451	0.0810	-0.1867
0.15	1.0000	0.0048	-0.0126	1.0000	0.0152	-0.0398	1.0019	0.0481	-0.1254	1.1503	0.1549	-0.3311
0.20	1.0000	0.0126	-0.0366	1.0002	0.0399	-0.1156	1.0156	0.1264	-0.3573	1.7130	0.3671	-0.7074
0.25	1.0000	0.0253	-0.0820	1.0008	0.0800	-0.2591	1.0688	0.2519	-0.7502	2.6378	0.2746	-1.1383
0.30	1.0000	0.0426	-0.1558	1.0028	0.1347	-0.4911	1.1927	0.3870	-1.2627	3.8682	0.1253	-1.5834
0.40	1.0001	0.0821	-0.4098	1.0176	0.2535	-1.2724	1.6680	0.2766	-2.4407	5.5656	0.1701	-2.3219
0.50	1.0007	0.1064	-0.8164	1.0626	0.2940	-2.4508	2.3008	0.1256	-3.6158	6.2345	0.3001	-2.9026
0.65	1.0059	0.0714	-1.7062	1.2232	0.1298	-4.6649	2.9228	0.1576	-5.2569	6.5275	0.5943	-3.8731
0.80	1.0121	0.0372	-2.8205	1.4070	0.0856	-6.9093	3.1830	0.2720	-6.7173	6.5476	1.0193	-4.6378
1.0	1.0169	0.0257	-4.4062	1.5813	0.1075	-9.5728	3.3003	0.6150	-8.3070	6.4521	1.6091	-5.5655
1.1	1.0284	0.0242	-5.0804	1.6319	0.1269	-10.705	3.3043	0.7291	-9.3707	3.9938	1.9723	-5.7822
1.5	1.0380	0.0294	-7.1351	1.6895	0.3139	-14.188	3.2595	1.7858	-12.431	6.1953	3.2343	-7.1843
2.0	1.0300	0.0346	-8.2681	1.6543	0.7002	-16.943	3.1129	4.1335	-14.861	5.8580	5.0176	-9.1910
3.0	1.0219	0.0359	-8.8802	1.5541	0.8865	-21.120	2.8569	6.2368	-20.175	5.2735	8.3522	-12.357
4.0	1.0166	0.0348	-8.9100	1.4737	0.9054	-23.585	2.6777	6.7880	-23.911	4.9251	10.154	-15.459
6.0	1.0111	0.0349	-8.9180	1.3619	0.9048	-26.615	2.4372	6.1401	-30.983	4.4537	12.523	-22.661
10.0	1.0093	0.0320	-8.9538	1.2417	0.8179	-29.150	2.1787	5.9436	-42.350	3.9638	15.174	-32.967
15.0	1.0055	0.0331	-8.9412	1.1633	0.8666	-29.569	1.9800	6.0664	-51.579	3.5630	18.246	-42.278
30.0	1.0035	0.0369	-8.9488	1.0833	0.7957	-29.981	1.6771	5.8287	-69.931	2.9913	18.790	-65.764
50.0	1.0013	0.0240	-8.9672	1.0486	0.8253	-29.593	1.4800	5.7678	-81.971	2.6156	19.648	-90.552
100.0	1.0007	0.0053	-8.9248	1.0243	0.9387	-29.537	1.2642	6.2041	-91.150	2.2026	19.993	-133.37

Table 4
Constants in Eq. (13)

R	a	b	A_{max}
0.33	4.5486	16.2362	1.6541
0.50	1.0007	29.1824	1.0001
1.00	5.8133	19.4021	1.7704

the top of the vertical wall (i.e., $Y/H = 1$), due to the impingement of the rising plume near this point.

4.2. Effect of aspect ratio on velocity and flow field

Variations of vertical velocity at $Y = 0.5$ are presented in Fig. 4 with $R = 0.33$, 0.5, and 1. At $R = 1$, because only uni-cellular flow exists in the enclosure, the flow patterns are similar to those in the regular natural convection systems. The velocity profiles are shown to be skew-symmetric with respect to the enclosure centerline (Fig. 4(a)).

For the case of $R = 0.5$, the maximum density line and the enclosure centerline coincide. A pair of roll cells is generated symmetrically in the rectangular enclosure. The velocity profiles show an M shape with two peaks near the vertical walls and one valley at the centerline (Fig. 4(b)).

As $R = 0.33$, the maximum density line shifts close to the cold wall and the convective flow mainly initiates from the hot wall. It can be observed from Fig. 4(a), while the velocity profile near the hot wall (left) displays similar behavior with that in Fig. 4(b), it exposes more complex features near the cold wall (right) due the strong impact of the main convective flow cell.

4.3. Effect of aspect ratio on interaction between maximum and minimum stream functions

The convective flow fields can be presented in terms of the stream function, which is defined as

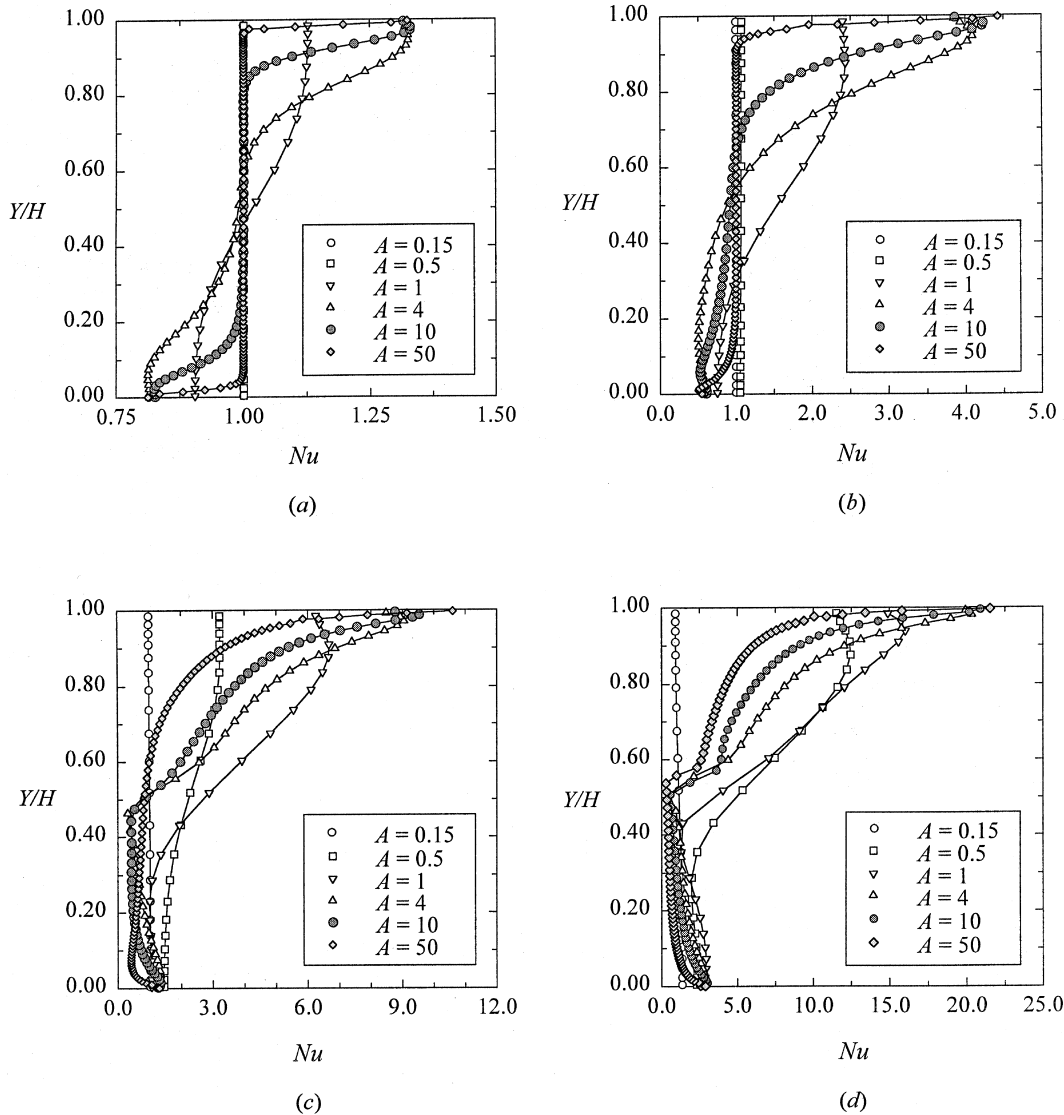$$u = \frac{\partial \psi}{\partial y}, \quad v = -\frac{\partial \psi}{\partial x}. \tag{16}$$

Fig. 3. Distributions of local Nusselt number along cold vertical walls at $R = 0.33$: Ra $= 10^3$; Ra $= 10^4$; Ra $= 10^5$; Ra $= 10^6$.
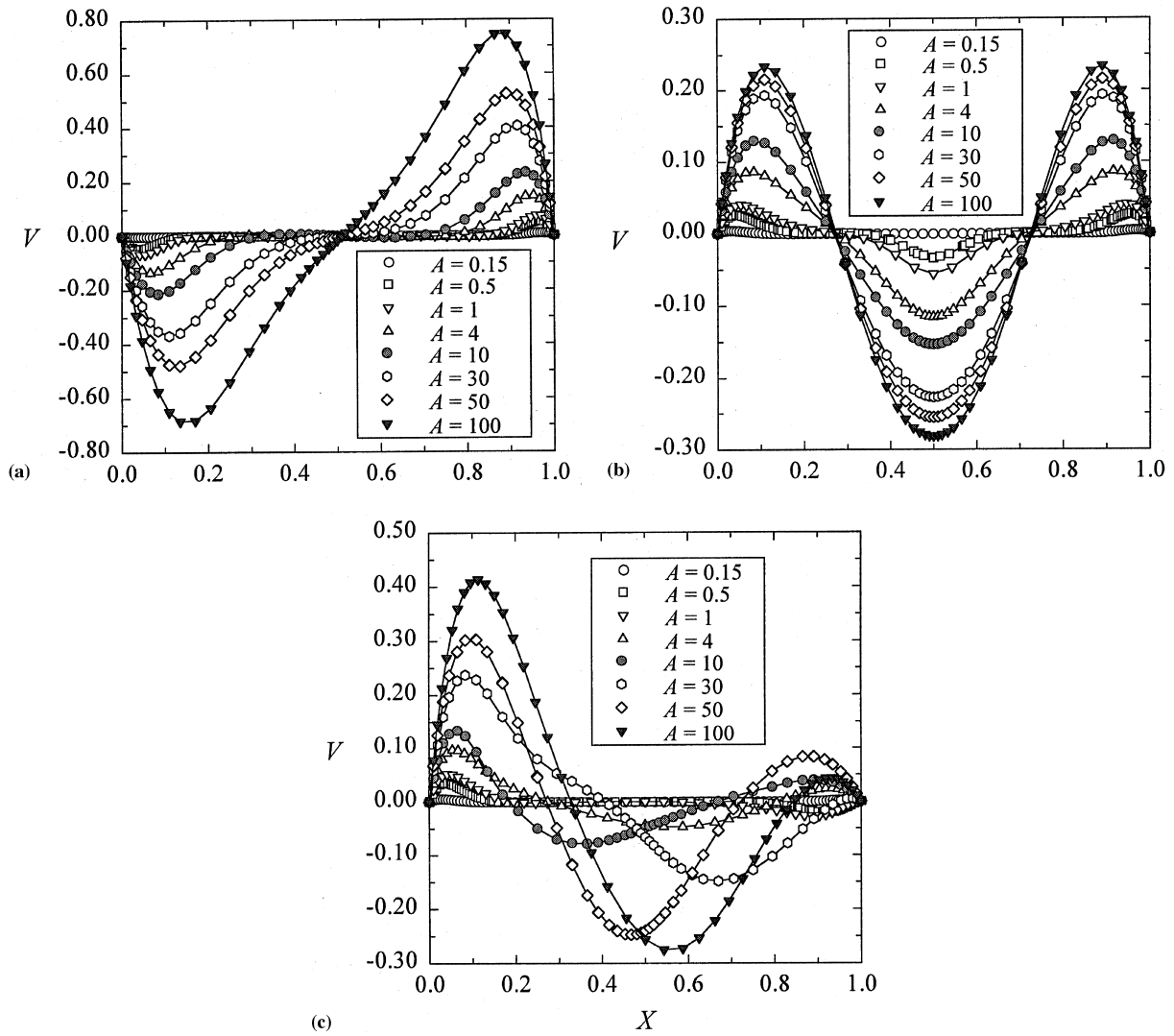
Fig. 4. Vertical velocity components profiles at $Y = 0.5$ for $\mathrm{Ra} = 10^6$: (a) $R = 1$; (b) $R = 0.5$; (c) $R = 0.33$.

The dimensionless stream function is defined as $\Psi = \psi/(\kappa\sqrt{\mathrm{Ra}\,\mathrm{Pr}})$.

The ratio of $\Psi_{\mathrm{inv}}/|\Psi_{\mathrm{reg}}|$ is introduced to provide a quantitative description of the interaction between inversional and regular convection in an enclosure, where Ψ_{inv} and Ψ_{reg} are associated with anti-clockwise rotating cells (developed from the cold wall as inversional convection) and clockwise rotating cells (developed from the hot wall as regular convection) in this problem. For the case of $R = 1$, since only regular convection exists, $\Psi_{\mathrm{inv}}/|\Psi_{\mathrm{reg}}| \equiv 0$. For symmetric density gradient cases (i.e., $R = 0.5$), $\Psi_{\mathrm{inv}}/|\Psi_{\mathrm{reg}}| \equiv 1$.

The variations of $\Psi_{\mathrm{inv}}/|\Psi_{\mathrm{reg}}|$ versus A at $R = 0.33$ and different Ra values are displayed in Fig. 5. For low Ra, $\Psi_{\mathrm{inv}}/|\Psi_{\mathrm{reg}}|$ approaches its local maximum as $A \to 0$, and decreases sharply as $A \to 1$. As A becomes very large, the stream function ratio approaches a constant. Increasing Ra above 10^4, a peak protrudes and develops on the $\Psi_{\mathrm{inv}}/|\Psi_{\mathrm{reg}}|$ curve in the regime near $A = 3$, indicating inversional convection is greatly enhanced.

Numerical results show that as $\mathrm{Ra} > 4 \times 10^5$ the peak near $A = 3$ exceeds those at small A. While the maximum of $\Psi_{\mathrm{inv}}/|\Psi_{\mathrm{reg}}|$ occurs either at small A or $A = 3$, depending on Ra, the
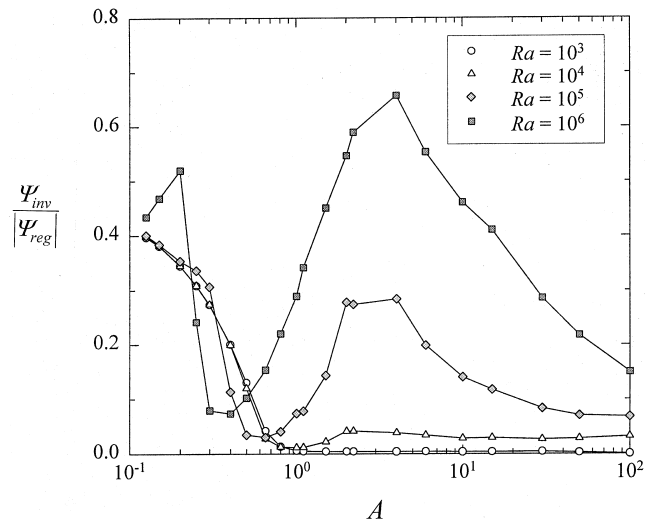
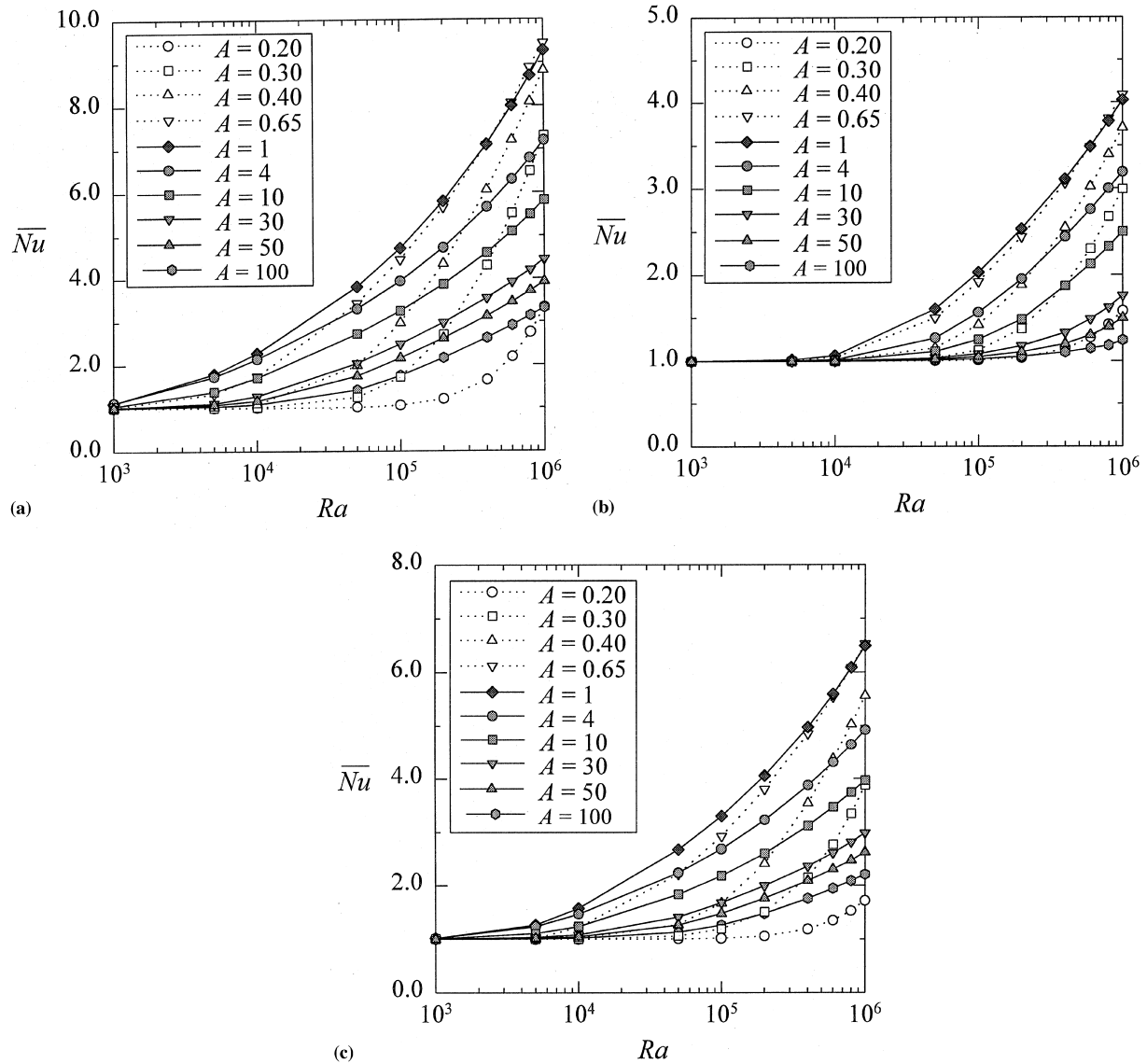Fig. 5. Aspect ratio effect on $\Psi_{\mathrm{inv}}/|\Psi_{\mathrm{reg}}|$ for $R = 0.33$.

Fig. 6. Aspect ratio effect on $\overline{Nu}$–Ra behavior: (a) $R = 1$; (b) $R = 0.5$; (c) $R = 0.33$.

minimum $\Psi_{inv}/|\Psi_{reg}|$ is seen to appear in the range $0.4 < A < 1$, depending on Ra values.

4.4. Effect of aspect ratio on $\overline{Nu}$–Ra behavior

The onset of convection in an enclosure is referred to as thermal instability. The critical Rayleigh number Ra_c is defined as the number at which a convective flow initiates. It is believed that thermal instability is generally associated with Rayleigh–Bénard convection. However, it has been found from this study that thermal instability could be also associated with natural convection in density inversion fluids, especially for large thermal resistance cases (e.g., $R = 0.5$, see Fig. 6(b)).

As seen from Fig. 6, the $\overline{Nu}$–Ra behaviors are strongly affected by the aspect ratio A and density distribution parameter R. The aspect ratio effect is seen to be significant for $R = 1$ and $R = 0.33$ but moderate for $R = 0.5$. The difference of the $\overline{Nu}$–Ra behavior between $A < 1$ and $A \geqslant 1$ can be easily seen in Fig. 6(a) and (c). For $A < 1$ $\overline{Nu}$ increases slowly at low Ra and steeply at high Ra. By contrast, for $A \geqslant 1$ the $\overline{Nu}$–Ra

curves display more smoothly. This may be explained as following: with a very thin water layer ($A < 1$), the effective buoyancy force is too weak to initiate convective flow and thus, its corresponding Ra_c is quite high. In a narrow vertical enclosure where $A \gg 1$, buoyancy force effect becomes so strong that Ra_c cannot be observed. In all cases, as soon as the convective flow starts, it will continue to develop with the increasing Ra. For symmetric density gradient cases, Ra_c gets rather large, near 10^4 for most aspect ratios (Fig. 6(b)), reflecting the large thermal resistance introduced between the two-roll cell interface.

The computed $\overline{Nu}$ values from the present work have been compared with available data in the literature (Table 5). Though Lin and Nansteel (1987) employed different density-temperature correlation, the relative difference between two results is less than 0.9%. Reasonably good agreement is observed between experimental (1995) and computational data, with relative difference at $1.14 \sim 5.18\%$. It is interesting to note that even though De Vahl Davis (1983) data were based on air (Pr = 0.73), the relative difference with the present results is only about 5%.

Table 5
Comparison of $\overline{Nu}$ between the present study and other investigations ($A = 1$)

Ra	$R = 0.5$			$R = 1$		
	Present study	Lin and Nansteel (1987)	Elkouh and Baliga (1995)[a]	Present study	Lin and Nansteel (1987)	De Vahl Davis (1983)[b]
10^3	1.0007	1.0009		1.1186	1.119	1.116
10^4	1.0655	1.076		2.2739	2.278	2.234
10^5	2.0298	2.080		4.7143	4.709	4.487
10^6	4.0272	4.090	4.236	9.2742	9.195	8.811
			4.086			

[a] Experimental data.
[b] For air flow and $Pr = 0.73$.

5. Conclusions

A finite element analysis has been performed to evaluate the aspect ratio effect on convective flow and heat transfer in water subjected to density inversion in rectangular enclosures. Numerical results reveal that the mean Nusselt number $\overline{Nu}$ exhibits a strong dependence on the aspect ratio A, the Rayleigh number Ra, and the density distribution parameter R. If the aspect ratio is very small, the heat transport across a vertical wall diminishes due to the decrease of the effective buoyancy force. By contrast, for a large aspect ratio the heat transfer rate also decreases due to the enhanced shear stress effect. As A approaches infinity, all $\overline{Nu}$–A curves asymptotically approach unity. Based on the numerical results, a new correlation is developed to predict the maximum mean Nusselt number under different A and R values. The $\overline{Nu}$–Ra curves exhibit essentially the different behaviors for $A < 1$ and $A \geqslant 1$.

The stream function ratio $\Psi_{inv}/|\Psi_{reg}|$ is used to present the interaction between regular and inversional convective flows in an enclosure. For the symmetric density gradient cases (where $R = 0.5$), $\Psi_{inv}/|\Psi_{reg}| \equiv 1$. For $R = 0.33$, as Ra is small, the enhancement of the density inversion effect is found to occur at small A; at large Ra, a peak on the $\Psi_{inv}/|\Psi_{reg}|$ curves develops in the regime near $A = 3$. In such circumstances, both the density inversing effect and regular effective buoyancy effect determine heat transfer characteristics of convective flows.

References

Delber, W.R., 1966. On the analogy between thermal and rotational hydrodynamic stability. J. Fluid Mech. 24, 165–176.

De Vahl Davis, G., 1983. Natural convection on air in a square cavity – a bench mark numerical solution. Int. J. Numer. Fluids 3, 249–264.

Elkouh, N., Baliga, B.R., 1995. Effect of variable properties on natural convection in water near its density inversion temperature. HTD-Vol. 33, 53–63.

Fluid Dynamics International, 1995. FIDAP User's manual, Version 7.5.

Fujii, T., 1974. Fundamentals of free convection heat transfer. Prog. Heat Tran. Engr. 3, 66–67.

Gebhart, B., Mollenderf, J.C., 1977. A new density relation for pure and saline water. Deep-Sea Res. 24, 831–848.

Goren, S.L., 1966. On free convection in water at 4°C. Chem. Engrg. Sci. 21, 515–518.

Ivey, G.N., Hamblin, P.F., 1989. Convection near the temperature of maximum density for high Rayleigh number, low aspect ratio, rectangular cavities. ASME J. Heat Transfer 111, 100–105.

Kell, G.S., Whalley, E., 1975. Reanalysis of the density of liquid water in the range 0–150°C and 0–1 K bar. J. Chem. Phys. 62, 3496–3503.

Lankford, K.E., Bejan, A., 1986. Natural convection in a vertical enclosure filled with water near 4°C. ASME J. Heat Transfer 108, 763–775.

Lin, D.S., Nansteel, M.W., 1987. Natural convection heat transfer in a square enclosure containing water near its density maximum. Int. J. Heat Mass Transfer 30, 2319–2329.

McDonough, M.W., Faghri, A., 1994. Experimental and numerical analyses of the natural convection of water through its density maximum in a rectangular enclosure. Int. J. Heat Mass Transfer 37, 783–801.

Robillard, L., Vasseur, P., 1981. Transient natural convection heat transfer of water with maximum density effect and supercooling. ASME J. Heat Transfer 103, 528–534.

Robillard, L., Vasseur, P., 1982. Convective response of mass of water near 4°C to a constant cooling rate applied on its boundaries. J. Fluid Mech. 118, 123–141.

Seki, N., Fukusako, S., Inaba, H., 1978. Free convective heat transfer with density inversion in a confined rectangular vessel. Wärme- und Stuffübertragung 11, 145–156.

Sun, Z.-S., Tien, C., Yen, Y.-C., 1969. Thermal instability of a horizontal layer of liquid with maximum density. AIChE J. 15, 910–915.

Tong, W., Koster, J.N., 1993. Natural convection of water in a rectangular cavity including density inversion. Int. J. Heat Fluid Flow 14, 366–375.

Tong, W., Koster, J.N., 1994. Density inversion effect on transient natural convection in a rectangular enclosure. Int. J. Heat Mass Transfer 37, 927–938.

Wagenbreth, H., Blanke, H., 1971. Die Dichte des Wassers im internationalen Einheitensystem und in der internationalen Praktischen Temperaturskala von 1968. PTB-Mitteilungen 6, 412–415.

Watson, A., 1972. The effect of the inversion temperature on the convection of water in an enclosure rectangular. Quart. J. Mech. Appl. Math. 25, 423–446.